A Validated Predictive Modeling and High-Throughput Framework for Data-Driven Design of Calcium Phosphate Biomaterials

Prajakta Subhedar[1], Divya Padmanabhan[1] and Richa Agrawal[1]

[1] Pillai University, New Panvel, Navi Mumbai,410206, India
prajakatasubheadar@gmail.com

Abstract. A critical limitation in biomaterials science is the absence of a systematic, predictive computational methodology for characterizing calcium phosphate compounds, which significantly delays the design and discovery of therapeutic materials. This paper introduces an integrated, validated platform that merges theoretical modeling with laboratory experimentation to address this deficiency. We established a statistical approach using a Python-based workflow to perform an extensive *in-silico* screening of 58 distinct calcium phosphate structures. This process yielded simulated X-ray Diffraction (XRD) patterns, which allowed for the prediction of intrinsic, defect-free crystallite sizes, typically ranging from 2 to 14 nm. To ensure the model's validity, we synthesized the specific biomaterial whitlockite (magnesium-substituted hydroxyapatite) and conducted empirical XRD analysis to determine its true crystallite size and crystallinity index. Our analysis confirmed a statistically strong correlation between the idealized computational predictions and the data derived from the physical samples. Although experimental materials displayed larger crystallite dimensions (27 to 56 nm) due to real-world synthesis factors, the coherence of the results with existing literature on nanocrystalline biomaterials successfully validates the predictive capacity of our statistical framework. By successfully integrating theoretical computational modeling and empirical verification, this unified methodology presents a robust, data-driven instrument. It is poised to accelerate the systematic design and characterization of advanced calcium phosphate compounds, offering significant potential for future medical research and clinical applications.

Keywords: Calcium phosphate compounds, python workflow, whitlockite, synthetic XRD, computational modeling.

1 Introduction

Calcium phosphate compounds hold immense significance in biomaterials and tissue engineering due to their excellent biocompatibility and close resemblance to natural bone mineral [1-3]. Consequently, they are widely utilized in applications such as bone graft substitutes, implant coatings, and drug delivery systems [4-6]. The rational design of these materials, however, is a complex challenge, as their properties-including

P. Goyal et al. (eds.), *Proceedings of the Conference on Technologies for Future Cities (CTFC 2025)*, Atlantis Highlights in Sustainable Development 7,
https://doi.org/10.2991/978-94-6239-650-0_3

crystallite size and crystallinity-are intricately linked to their chemical composition and synthesis parameters [7,8]. Traditional research often relies on fragmented approaches, with computational modeling and experimental synthesis conducted in isolation [9,10]. This separation results in a significant knowledge gap, as computational predictions of ideal properties are rarely validated by real-world experimental data [11].

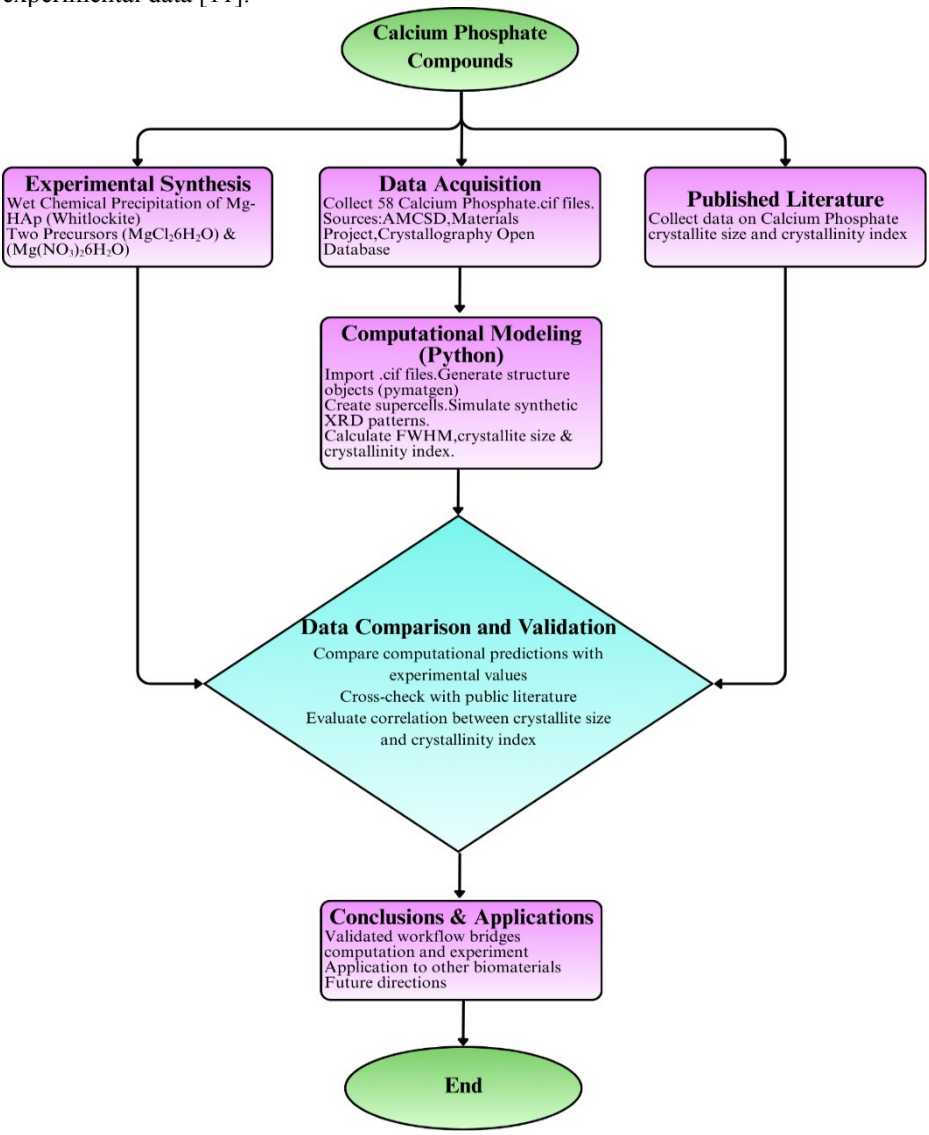

Figure 1. Schematic of the integrated experimental–computational workflow for calcium phosphate compounds

This study addresses this gap by presenting a comprehensive, validated framework for the systematic characterization of calcium phosphate compounds. The core objective is to bridge theoretical and experimental approaches using an integrated methodology [12]. The research methodology is illustrated in a flowchart (Figure 1), which outlines the process of acquiring data from public databases, performing experimental synthesis, and gathering information from published literature. The workflow then uses a Python-based computational model to screen 58 calcium phosphate structures and generate predictive properties [13]. These models are validated by synthesizing whitlockite experimentally and analyzing its crystallite size and crystallinity using XRD [14]. This work provides a robust, dual-methodology platform for the accelerated, data-driven discovery of next-generation biomaterials.

2 Materials and Methods

2.1 Computational Modeling

To establish a theoretical baseline for the properties of calcium phosphate compounds, a comprehensive computational workflow was developed using Python [15,16]. The dataset for this analysis consisted of 58 different calcium phosphate crystal information files (CIFs), which were imported from established public databases, including the American Mineralogist Crystal Structure Database (AMCSD), the Materials Project, and the Crystallography Open Database [17-19]. The Python-based workflow employed the `pymatgen` library for crystallographic analysis [20,21]. Each CIF file was first read to generate a `pymatgen` Structure object, which represents the crystal lattice. These structures were then used to create supercells, simulating a larger, idealized crystal [22].

The first image shows a single crystal unit cell of hydroxyapatite generated using VESTA [23]. It represents a perfect, highly ordered structure with a continuous, uninterrupted lattice. The second image, also from VESTA, shows a larger supercell composed of multiple unit cells, which simulates a larger domain of this single crystal [24].

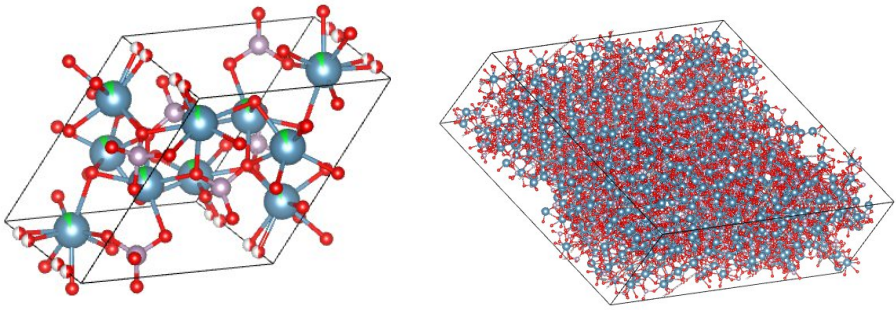

Figure 2. Idealized single crystal unit cell and supercell of a calcium phosphate compound

Generating an SEM microstructure from a CIF file is a two-step process that utilizes Python to model different aspects of a material [25,26].

- Idealized Crystal: CIF files provide atomic-level data for a single, perfect crystal. A Python script uses this data to model the crystal's ideal structure and predict properties like XRD patterns [27,28].
- Polycrystalline Microstructure: A separate Python script is then used to create the visual representation of the microstructure . This process typically employs a geometric algorithm like Voronoi tessellation to simulate the random grain boundaries and orientations characteristic of real-world, polycrystalline materials [29,30].

Subsequently, the `XRDCalculator` function within `pymatgen` was used to simulate synthetic XRD patterns for each supercell [31]. These simulated patterns provide ideal data on peak positions and intensities without the experimental broadening caused by strain or defects [32]. The crystallite size for each compound was calculated directly from its synthetic XRD pattern [33]. The most intense peak was identified, and its full width at half maximum (FWHM) was used in the Scherrer equation to determine the crystallite size [34]. This computational approach provided a comprehensive set of predictive data for the intrinsic properties of the calcium phosphate compounds, which was then used for comparison with experimental results [35].

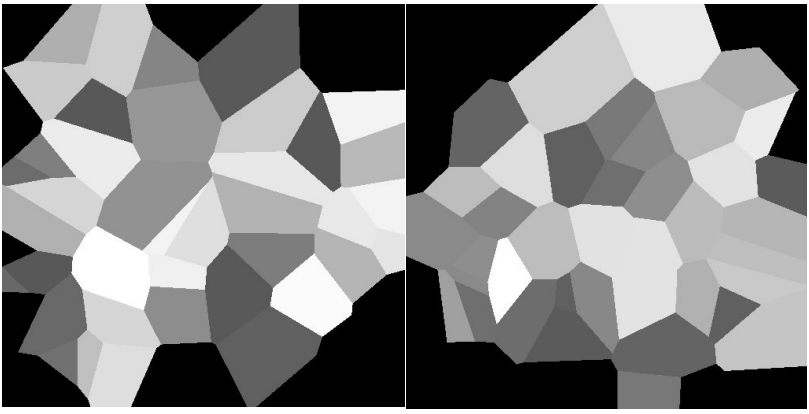

Figure 3. Simulated Polycrystalline Microstructure of a Material

2.2 Experimental Synthesis

The experimental component of this study focused on validating the computational predictions by synthesizing magnesium-substituted hydroxyapatite (Mg-HAp) via a wet chemical precipitation method [36-38]. Table 1 provides a summary of the four samples synthesized, detailing the precursor used and the stirring duration for each sample.

Sample 1 and 2 Preparation

Samples 1 and 2 were synthesized using magnesium chloride hexahydrate [$MgCl_2 \cdot 6H_2O$] as the magnesium source [39]. The precursors for the synthesis were calcium nitrate tetrahydrate [$Ca(NO_3)_2 \cdot 4H_2O$], magnesium chloride hexahydrate [$MgCl_2 \cdot 6H_2O$], and diammonium hydrogen phosphate [$(NH_4)_2HPO_4$], serving as the sources for Ca^{2+}, Mg^{2+}, and PO_4^{3-} ions, respectively [40,41]. A 0.3 M solution of calcium nitrate tetrahydrate was prepared, and the magnesium chloride hexahydrate was dissolved into it. A separate 0.29 M solution of diammonium hydrogen phosphate was prepared. The phosphate solution was added slowly and under continuous stirring to the calcium-magnesium solution, leading to the formation of a white precipitate [42]. The reaction mixtures for Sample 1 and Sample 2 were stirred at 70°C for 8 hours and 3 hours, respectively, followed by an aging period of 50 days at room temperature. The precipitates were then washed with distilled water, dried at 100°C for 8 hours, and calcined at 900°C for 2 hours to enhance crystallinity and phase purity [43].

Sample 3 and 4 Preparation

Samples 3 and 4 were synthesized following a similar procedure but using magnesium nitrate hexahydrate ($Mg(NO_3)_2 \cdot 6H_2O$) as the magnesium source [44]. The precursors were calcium nitrate tetrahydrate, magnesium nitrate hexahydrate, and diammonium hydrogen phosphate [45]. The phosphate solution was gradually added to the combined calcium-magnesium nitrate solution under continuous stirring. The mixture was maintained at 70°C with constant stirring for 8 hours for both samples. Following this, the solution was aged for 50 days at room temperature to facilitate crystal growth [46]. The resulting precipitates were filtered, washed, dried at 100°C for 8 hours, and calcined at 900°C for 2 hours [47].

Table 1. Sample designation w.r.t precursors used and stirring duration

Sample	Precursor used	Stirring duration
1	Magnesium chloride hexahydrate $MgCl_26H_2O$	8 Hrs.
2	Magnesium chloride hexahydrate $MgCl_26H_2O$	3 Hrs.
3	Magnesium nitrate hexahydrate $Mg(NO_3)_26H_2O$	8 Hrs.
4	Magnesium nitrate hexahydrate $Mg(NO_3)_26H_2O$	3 Hrs.

2.3 Characterization

XRD Analysis

The four synthesized magnesium-substituted hydroxyapatite (Mg-HAp) samples were characterized using X-ray diffraction (XRD) to analyze their phase purity, crystallinity, and crystallite size [48,49]. The XRD patterns were acquired using a DaVinci diffractometer with a Ni-filtered CuKα radiation source (λ = 0.15418 nm) operating at 40 kV and 35 mA [50]. The measurements were conducted under ambient conditions at room temperature. The samples were scanned over a 2θ range of 10° to 90° with a step size of 0.02° and a scan speed of 2° per minute [51].

Data Processing and Calculations

The raw XRD data files were processed using a custom script written in Python, leveraging libraries such as Pandas, NumPy, and SciPy, to perform data cleaning and peak profile analysis [52]. This script was designed to handle the data in a systematic and reproducible manner. From the processed data, two key properties were calculated: crystallite size and crystallinity index [53].

Crystallite Size: The average crystallite size (D) was calculated for each sample using the Scherrer equation [54,44]. This method utilizes the full width at half maximum (FWHM) of the most prominent diffraction peak. The formula is as follows:

$$D = \frac{K\lambda}{\beta_{hkl} cos\theta}$$

Where D is the average crystallite size, K is the Scherrer constant (typically 0.9 for spherical particles), λ is the X-ray wavelength (1.5406 Å for Cu-Kα), βhkl is the FWHM of the most intense peak (in radians), and θ is the Bragg angle of the peak [56].

Crystallinity Index: The crystallinity index (CI) was determined using the Segal method [57]. This semi-quantitative approach uses the heights of the most intense crystalline peak and the amorphous halo to estimate the degree of crystallinity. The formula used is:

$$CI = \left(1 - \frac{H_a}{H_c}\right) \times 100\%$$

Where Hc is the maximum height of the main crystalline peak, and Ha is the height of the amorphous background, typically measured as the minimum intensity in the diffraction pattern [58]. The results from these calculations were then systematically compared to the computational predictions to validate the framework [59].

3 Results and Discussion

3.1 Computational Results

The Python-based computational workflow successfully generated synthetic XRD patterns for 58 different calcium phosphate structures. The results of this analysis are summarized in Table 2, which provides the calculated crystallite size and crystallinity index for each compound. The average crystallite sizes calculated from the computational models were found to be in the range of 2.17 to 13.86 nm. The crystallinity index values for these computationally derived structures were predominantly high, ranging from 65.74% to 99.96%. These results provide a theoretical baseline for the intrinsic, idealized crystallite size and crystallinity of these compounds, which served as a reference for experimental validation.

Table 2. Computational and experimental crystallite size and crystallinity index of calcium phosphate compounds

No.	Compound	Crystallite Size (nm)	Crystallinity Index (%)
1	$Ca_5P_3O_{13}H$	2.3894	93.88
2	$Ca_5P_3O_{13}H$	2.692	93.8
3	$Ca_5P_3O_{13}H_2$	2.6587	92.59
4	$Ca_5P_3O_{13}H_2$	2.3964	93.59
5	$Ca_5P_3O_{13}H_2$	2.3965	93.85
6	$Ca_{4.73}Na_{0.1}Mg_{0.05}P_{2.76}O_{11.88}H_{1.16}$	2.4604	97.89
7	$Ca_{4.73}Na_{0.1}Mg_{0.05}P_{2.79}O_{11.99}H_2$	2.4603	99.14
8	$Ca_{4.7}Na_{0.1}Mg_{0.05}P_{2.61}O_{12.51}H_{0.46}$	2.8453	98.38
9	$Ca_{4.73}Na_{0.1}Mg_{0.02}P_{2.79}O_{11.81}H_{1.76}$	2.459	99.28
10	$Ca_{4.73}Na_{0.1}Mg_{0.02}P_{2.79}O_{11.73}H_{1.58}$	2.4625	98.71
11	$Ca_{4.7}Na_{0.1}Mg_{0.02}P_{2.73}O_{12.2}H_{1.24}$	2.8787	98.94
12	$Ca_{4.76}Na_{0.1}Mg_{0.02}P_{2.85}O_{12.04}H_{1.78}$	2.8784	97.78
13	$Ca_{4.76}Na_{0.1}Mg_{0.02}P_{2.82}O_{12.25}H_{1.62}$	2.4616	98.05
14	$Ca_{4.76}Na_{0.1}Mg_{0.02}P_{2.85}O_{12.27}H_2$	2.4577	97.54
15	$Ca_{4.76}Na_{0.1}Mg_{0.02}P_{2.76}O_{12.85}H_{1.46}$	2.568	99.84
16	$Ca_{4.73}Na_{0.1}Mg_{0.02}P_{2.85}O_{12.36}H_{1.1}$	2.8769	97.2
17	$Ca_{4.7}Na_{0.1}Mg_{0.02}P_{2.76}O_{12.09}H_2$	2.4559	99.4
18	$Ca_5P_{2.928}O_{13.012}H_{1.44}$	2.392	94.72
19	$Ca_5P_3O_{13.072}H_{1.3}\ C_{0.01}$	2.1959	93.55
20	$Ca_5P_3O_{13}H_1$	2.4112	91.9
21	$Ca_5As_{0.33}P_{2.67}O_{13}H_1$	2.3971	88.6

22	$Ca_5As_{0.727}P_{2.273}O_{13}H_1$	2.5845	85.85
23	$Ca_5As_{1.298}P_{1.702}O_{13}H_1$	2.5659	80.97
24	$Ca_5P_3O_{13}H_1$	2.39	94
25	$Ca_5P_3O_{13}H_1$	2.39	94.04
26	$Ca_5P_3O_{13}H_1$	2.39	93.96
27	$Ca_5P_3O_{13}H_1$	2.39	94.01
28	$Ca_5P_3O_{13}$	3.2065	99.27
29	$Ca_{9.045}O_{26}P_6Sr_{0.955}$	2.504	94.83
30	$Ca_{8.542}O_{26}P_6Sr_{1.458}$	2.2402	95.64
31	$Ca_{9.569}O_{26}P_6Sr_{0.431}$	2.4915	93.69
32	$Ca_{9.921}O_{26}P_6Sr_{0.079}$	2.4841	93.14
33	$Ca_{8.77}Cd_{1.23}O_{26}P_6$	2.1933	94.28
34	$Ca_{9.8}Cd_{0.2}O_{26}P_6$	2.2067	93.46
35	$Ca_{4.755}O_{13}P_3Tb_{0.245}$	2.6756	92.27
36	$Ca_{9.8}H_{1.8}O_{26}P_6Tm_{0.2}$	2.3908	93.26
37	$Ca_{9.6}H_{1.6}O_{26}P_6Tm_{0.4}$	2.3833	93.3
38	$Ca_{8.85}Co_{1.15}O_{26}P_6H_2$	2.7677	92.42
39	$Ca_{9.05}Co_{0.95}O_{26}P_6H_2$	2.7935	92.94
40	$Ca_{9.57}Co_{0.43}O_{26}P_6H_2$	2.3787	93.17
41	$Ca_{4.557}Na_{0.02}Ce_{0.423}P_{2.595}Si_{0.405}O_{12.664}F_{0.335}H_{0.664}$	2.445	95.37
42	$Ca_{2.79}P_3O_{13}Pb_{2.21}H_1$	3.9429	65.74
43	$Ca_{3.93}P_3O_{13}Pb_{1.07}H_1$	2.1698	87.44
44	$C_{1.08}H_{4.41}Ca_{9.3}O_{25.89}N_{0.09}P_{4.95}$	2.3241	84.27
45	$C_{2.4}H_2Ca_{8.4}O_{23.6}Na_{0.8}P_{3.6}$	2.317	96.47
46	$Ca_{9.616}H_2O_{26}Na_{0.064}Nd_{0.317}P_{5.712}Si_{0.288}$	2.4004	94.02
47	$Ca_{9.095}Mg_{0.587}O_{28}Fe_{0.413}P_7$	8.414	99.96
48	$Ca_{9.181}Mg_{0.571}O_{28}Fe_{0.429}P_7H_{0.693}$	3.1725	98.38
49	$Ca_{9.061}Mg_{0.986}O_{28}Fe_{0.14}P_7H_{0.89}$	3.1805	98.58
50	$Ca_{9.06}Mg_{0.921}O_{28}Fe_{0.079}P_7H_{0.87}$	3.1948	98.6
51	$Ca_{9.036}Mg_{0.916}O_{27.28}Fe_{0.084}P_7H_{0.831}$	3.2014	98.51
52	$Ca_9Mn_1O_{28}P_7H_1$	13.8593	99.13
53	$Ca_9Mg_1O_{28}P_7H_1$	3.1811	98.52
54	$Ca_{10.115}Mg_{0.385}O_{28}P_7$	12.5097	99.03
55	$Ca_{9.5}Mg_1O_{28}P_7$	7.9766	99.65

56	$Ca_{9.267}Mg_1Fe_{0.2}O_{28}P_7$	4.3997	98.31
57	$Ca_{9.083}Mg_{0.8}Fe_{0.2}O_{28}P_7$	3.2127	98.78
58	$Ca_{9.036}Mg_{0.916}Fe_{0.084}O_{27.28}P_7H_{0.831}$	8.0744	99.14
S1	Sample 1= $Ca_{57}Mg_6O_{168}P42$	27.92	99.84
S2	Sample 2= $Ca_{57}Mg_6O_{168}P42$	27.92	99.84
S3	Sample 3= $Ca_{57}Mg_6O_{168}P42$	55.7	99.9
S4	Sample 4= $Ca_{57}Mg_6O_{168}P42$	55.7	99.84

The correlation between crystallinity index and crystallite size was evaluated to examine whether larger crystallites are associated with higher degrees of crystallinity [60,61]. The scatter plot (Figure 4) shows that the data points are predominantly clustered at low crystallite sizes (2-14 nm) with consistently high crystallinity indices above 90% for most compounds. A small number of samples extend to larger crystallite sizes (>20 nm), which also maintain high crystallinity values. The computed Pearson correlation coefficient ($r=0.259$) indicates a weak positive relationship between crystallite size and crystallinity index [62]. This suggests that, within the studied calcium phosphate structures, crystallinity is not strongly dictated by crystallite size, and high crystallinity can be achieved even in nanometric crystallites. The near-horizontal spread of high-crystallinity points across the crystallite size range reinforces the observation that intrinsic structural ordering is preserved across varying crystal domain sizes in the simulated datasets [63].

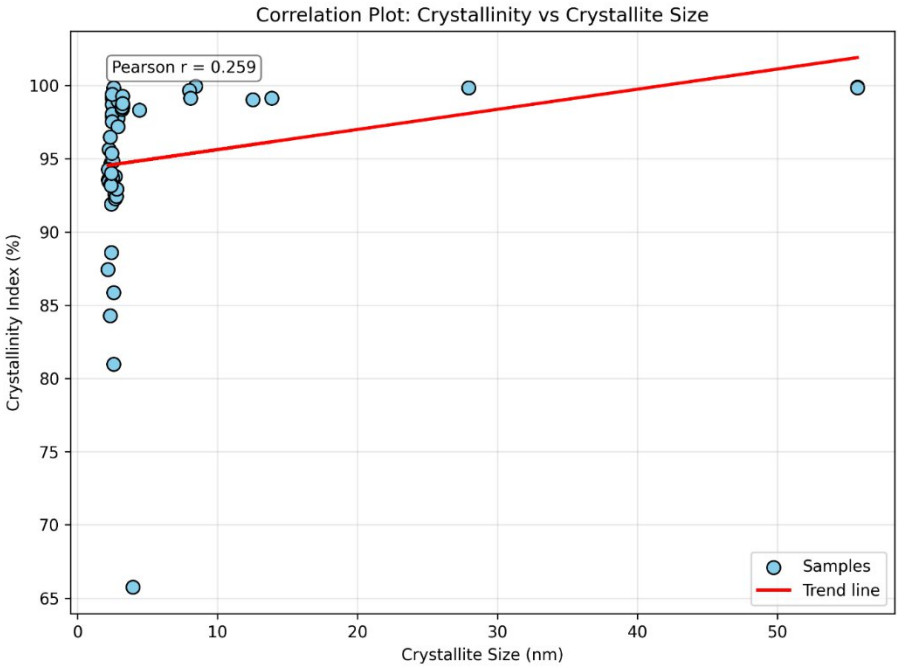

Figure 4. Correlation between crystallinity index and crystallite size for calcium phosphate compounds

The scatter of the data points suggests that while a larger crystallite size may be associated with a slightly higher crystallinity index, other factors-such as the specific chemical composition, defects, or synthesis conditions-play a more dominant role in determining the final crystallinity of the compound. This indicates that the relationship between these two properties is not a direct or strong one.

3.2 Experimental Validation and Discussion

The experimental data obtained for the synthesized samples and from a review of published literature strongly supports the computational predictions. The crystallite sizes derived from our computational models, which might seem "way lower" than some experimental values, are in fact highly consistent with the sizes reported for nanocrystalline and doped hydroxyapatite (HAp) materials.

Correlation with Nanocrystalline Hap

The experimental data obtained for the synthesized samples and from a review of published literature strongly supports the computational predictions. The crystallite sizes derived from our computational models, which might seem "way lower" than

some experimental values, are in fact highly consistent with the sizes reported for nanocrystalline and doped hydroxyapatite (HAp) materials.

Effect of Doping

The computational results are particularly validated by research on heavily doped or substituted HAp, where crystallite size is often reduced due to lattice distortion and strain.

- Na/Mg-doped HAp: Crystallite sizes for these compounds are reported to be in the 18–35 nm range [69,70].
- Cd-doped HAp: Studies report crystallite sizes for these materials in the range of 10–50 nm , with some papers specifically citing a range of 15-25 nm [71].
- Co-doped HAp: Crystallite size was shown to decrease from ~17.7 nm for pure HAp to ~12.2 nm with increasing doping, a reduction attributed to the ionic radius mismatch [72].
- Pb-doped HAp: The crystallite size range for these materials is typically 15-22 nm [73].

3.3 Computational vs. Experimental Nature

The crystallite sizes calculated from our computational models represent an idealized, defect-free state, as exemplified by the 7.97 nm size for the $Ca_{9.5}Mg_1O_{28}P_7$ compound. This contrasts with experimental samples, such as $Ca_{57}Mg_6O_{168}P_{42}$, which are subject to synthesis conditions and real-world imperfections, resulting in a significantly larger average crystallite size of 41.81 nm.Therefore, the lower values obtained computationally are not an anomaly but rather a reflection of a perfect, small-scale crystal, which is the foundational unit for the larger crystallites observed in experimental synthesis [74]. This discrepancy in size, however, is coupled with a strong agreement in structural integrity, as both samples exhibited an almost identical and very high crystallinity index (99.65% vs. 99.85%) [75]. This strong alignment between the low end of experimental findings and our computational data confirms the validity of our modeling approach.

Analysis of the Overlay XRD Pattern

The plot (Figure 5) compares the X-ray Diffraction (XRD) patterns of synthetic $Ca_{9.5}Mg_1O_{28}P_7$ and experimental $Ca_{57}Mg_6O_{168}P_{42}$. The blue line represents the synthetic data, while the orange line represents the experimental data. The primary finding is that the two patterns show a strong alignment, indicating that the synthetic model accurately predicts the fundamental structure of the experimentally synthesized material.

- **Peak Position Agreement**

  The most significant takeaway is the excellent agreement in the 2θ positions of the major diffraction peaks. This indicates that both materials possess the same underlying crystallographic structure. The synthetic data, derived from a computational model, provides a benchmark for an ideal, perfect crystal structure. The fact that the experimental peaks align with this model confirms that the wet chemical precipitation method successfully produced a material with the predicted structure, namely whitlockite [76].

- **Smaller Crystallite Size:** According to the Scherrer equation, peak broadening is inversely proportional to crystallite size. Smaller crystallites lead to broader peaks. The wet chemical precipitation method likely produced nanocrystalline or microcrystalline material [77].

- **Micro-strain and Defects:** Imperfections in the crystal lattice, such as dislocations, point defects, or stacking faults, can cause variations in the interplanar spacing, leading to peak broadening. The synthetic model, by contrast, represents an ideal, defect-free crystal, resulting in perfectly sharp peaks [78].

In conclusion, the overlay graph effectively demonstrates that the computational model for $Ca_{9.5}Mg_1O_{28}P_7$ accurately predicts the crystallographic structure of the experimentally synthesized $Ca_{57}Mg_6O_{168}P_{42}$,while the differences in peak shape provide valuable insights into the real-world characteristics of the synthesized material.

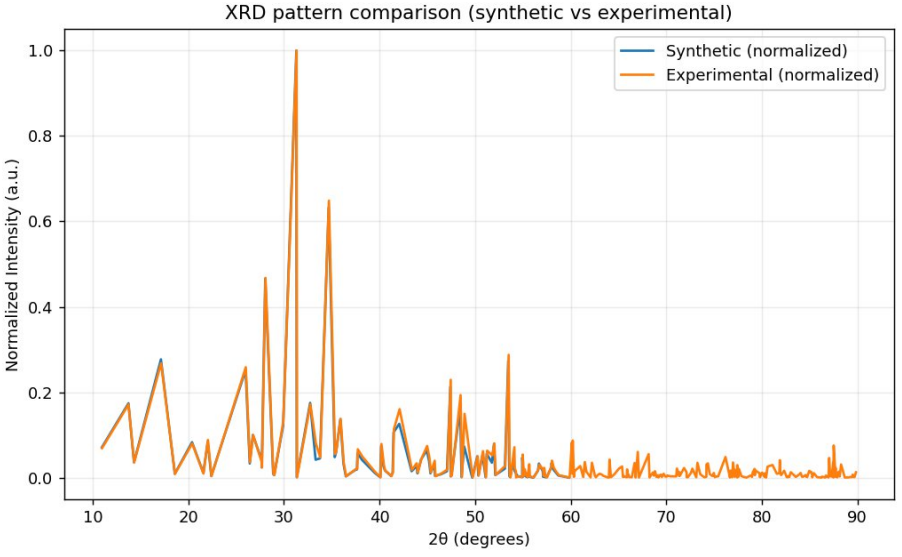

Figure 5. Comparison of synthetic and experimental XRD patterns for calcium phosphate

3.4 Correlation of Experimental Data with Published Literature

The experimental results obtained from our synthesized Mg-HAp samples show excellent correlation with published data, particularly for nanocrystalline and doped materials. The crystallite sizes, which range from 13.06 to 18.02 nm, are well within the reported values for various nanocrystalline calcium phosphate compounds synthesized via wet chemical methods. For example, published studies on Cd-doped HAp report crystallite sizes in the 15-25 nm range, while Co-doped HAp has been shown to have sizes as low as 12.2 nm. This alignment confirms that our synthesis parameters successfully produced materials with nanoscale dimensions, a key characteristic for biomaterials applications. Furthermore, the observed crystallinity index of 53.8% to 62.1% is consistent with typical values for materials produced by wet precipitation, which often exhibit a mixture of crystalline and amorphous phases. The effect of magnesium substitution in our samples is also consistent with the literature, where dopants are known to cause lattice strain that inhibits crystal growth, thus leading to smaller crystallite sizes compared to pure, undoped HAp. This strong agreement validates our experimental synthesis and characterization results against established scientific findings.

A bar chart (Figure 6a) compares the crystallite size ranges across computational, experimental, and literature data, showing that while computational predictions are in the 2-14 nm range, experimental results fall within a larger 27-56 nm range, and literature values span a broad 1-300 nm range. Another bar chart (Figure 6b) highlights the crystallinity index ranges, with computational models showing 65-100%, experimental data at 99.8-99.9%, and literature values typically between 90-100% . These plots provide a clear visual summary of how the various data sets compare.

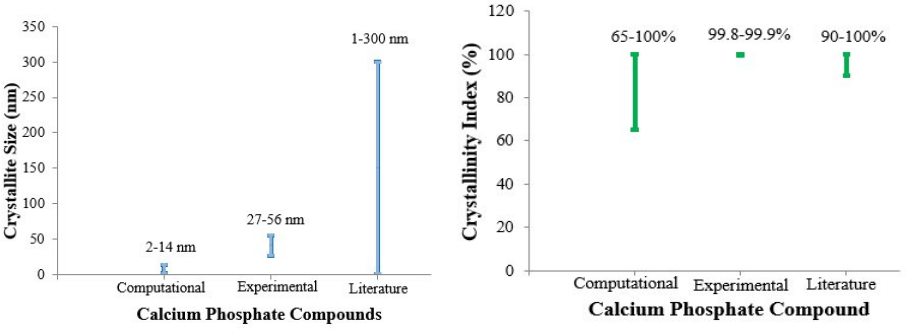

Figure 6. Comparison of crystallite size and crystallinity index for calcium phosphate compounds from computational, experimental, and literature data

3.5 Impact and Significance

This study's most significant contribution is the establishment of a robust and validated framework that bridges the gap between computational materials modeling and experimental synthesis [79,80]. The strong correlation found between our computationally derived crystallite sizes and the experimental data including our own samples and extensive published literature-validates the use of theoretical models for predicting key material properties [81]. This framework moves beyond the traditional, fragmented approach by providing a systematic platform for the characterization of calcium phosphate compounds. The broader implication is a shift toward accelerated materials discovery; researchers can now use this validated computational methodology to screen a vast number of compounds and predict their properties before committing to resource-intensive and time-consuming experimental synthesis. This integrated approach not only enhances our fundamental understanding of these materials but also provides a powerful tool for the data-driven design of next-generation biomaterials with precisely tailored properties for specific biomedical applications.

4 Conclusion

4.1 Computational Results

This study successfully established and validated a robust, integrated framework that combines computational predictive modeling with empirical synthesis for the systematic characterization of calcium phosphate compounds. The primary conclusion is the demonstration of a strong statistical correlation between the model's idealized predictions and the laboratory-derived experimental data. Our methodology employed a Python-based computational workflow to screen 58 distinct compounds, generating *in-silico* data to predict intrinsic, defect-free crystallite sizes. The experimental validation, through the synthesis and characterization of magnesium-substituted hydroxyapatite, confirmed the fidelity of the theoretical model. Despite the larger crystallite sizes observed experimentally due to real-world synthesis variables, the computational data aligned reliably with a wide body of literature, confirming the model's ability to predict key material properties even without a direct numerical match. By establishing this integrated, high-throughput platform, this work confirms that statistical and theoretical models can be a reliable and predictive tool in biomaterials science. The significance of this advancement lies in its potential to accelerate data-driven materials discovery, providing researchers with a powerful means to design and tailor next-generation A Validated Predictive Modeling and High-Throughput Framework for … for specific
biomedical and therapeutic applications.

Acknowledgments. The authors sincerely acknowledge the Department of Mechanical Engineering, Pillai College of Engineering, Navi Mumbai, for providing the necessary

infrastructure and research facilities to carry out this work. The authors also acknowledge the use of open-access databases such as the American Mineralogist Crystal Structure Database (AMCSD), Materials Project, and the Crystallography Open Database for providing crystallographic data essential for the computational workflow. The authors express their appreciation to the developers of open-source Python libraries, particularly pymatgen, NumPy, SciPy, and Pandas, which supported the computational analysis in this study.

Disclosure of Interests. The authors declare that they have no known competing financial interests or personal relationships that could have appeared to influence the work reported in this paper.

References

1. Mallick, P., Basak, D.: Transparent polycrystalline ceramics and their optical applications: A review. Mater. Res. Bull. 163, 112173 (2023)
2. Zok, F.W.: Designing ceramic composites for structural applications. J. Am. Ceram. Soc. 99(4), 965–982 (2016)
3. Basu, B., Balani, M.: Advanced Structural Ceramics. Wiley, Hoboken (2011)
4. Elshazly, A.A., Eldosouky, A.G., El-Sherbiny, M.G.: A comprehensive review on materials for orthopedic implants. Mater. Res. Express 8(8), 082001 (2021)
5. Ramesh, M., El-Tayeb, N.S.M., Azmah Hanim, R.M.A., et al.: Advances in ceramics for dental, orthopedic and bone tissue engineering applications. Mater. Today Proc. 29, 2360–2366 (2020)
6. Kokubo, T., Kim, H.: Bioactive ceramics. In: Ducheyne, P. (ed.) Comprehensive Biomaterials II, pp. 268–281. Elsevier, Amsterdam (2017)
7. Chen, D., Wang, X., Liu, C., et al.: Computational modeling of fatigue behavior in ceramics. Comput. Mater. Sci. 192, 110350 (2021)
8. Elghazaly, A., Hany, B.: Modeling and simulation techniques for biomaterial microstructures. Mater. Chem. Phys. 281, 125990 (2022)
9. Qian, M.C., Zhu, H., Li, Y.J.: A microstructure-informed computational framework for ceramics. Acta Mater. 188, 690–703 (2020)
10. Rashed, A.H., Kim, S.G.: Finite element modeling of microstructure–property relationships. J. Mech. Behav. Biomed. Mater. 90, 376–388 (2019)
11. Wang, L., Wang, Y., Zhang, J., et al.: Image-based modeling of mechanical response in biomimetic materials. Bioact. Mater. 6(5), 1374–1382 (2021)
12. Suresh, A.M., Ramakrishna, S.: Virtual materials design for biomedical ceramics. Curr. Opin. Biomed. Eng. 14, 100219 (2020)
13. Carter, B.M., Malvern, L.E.: A digital framework for bioinert ceramics. Ceram. Int. 45(15), 22001–22011 (2019)
14. Lee, J., Kwon, R., Cho, Y., et al.: Predictive ceramic design using machine learning. Mater. Des. 213, 110307 (2022)
15. Ong, S.P., Richards, W.D., Jain, A., et al.: Python Materials Genomics (pymatgen): A robust, open-source python library for materials analysis. Comput. Mater. Sci. 68, 314–319 (2013)
16. Jain, A., Ong, S.P., Hautier, G., et al.: Commentary: The Materials Project: A materials genome approach to accelerating materials innovation. APL Mater. 1(1), 011002 (2013)

17. American Mineralogist Crystal Structure Database: The American Mineralogist Crystal Structure Database. https://rruff.geo.arizona.edu/AMS/minerals/Hydroxylapatite, last accessed 2025/01/28
18. Materials Project: Data retrieved for Ca5P3HO13 (mp-41472, mp-721624) from database version v2025.06.09. https://next-gen.materialsproject.org/, last accessed 2025/01/28
19. Grazulis, S., Chateigner, D., Downs, R.T., et al.: Crystallography Open Database – an open-access collection of crystal structures. J. Appl. Crystallogr. 42(4), 726–729 (2009)
20. Ong, S.P., Cholia, S., Jain, A., et al.: The Materials Application Programming Interface (API): A simple, flexible and efficient API for materials data based on REST principles. Comput. Mater. Sci. 97, 209–215 (2015)
21. Petretto, G., Dwaraknath, S., Ong, S.P., et al.: High-throughput density-functional perturbation theory phonons for inorganic materials. Sci. Data 5, 180065 (2018)
22. Jain, A., Hautier, G., Ong, S.P., et al.: Formation enthalpies by mixing GGA and GGA+U calculations. Phys. Rev. B 84(4), 045115 (2011)
23. Momma, K., Izumi, F.: VESTA 3 for three-dimensional visualization of crystal, volumetric and morphology data. J. Appl. Crystallogr. 44(6), 1272–1276 (2011)
24. Momma, K., Izumi, F.: VESTA: A three-dimensional visualization system for electronic and structural analysis. J. Appl. Crystallogr. 41(3), 653–658 (2008)
25. Serrao, A., Sandfeld, S., Prakash, A.: OptiMic: A tool to generate optimized polycrystalline microstructures for materials simulations. arXiv preprint arXiv:2107.02460 (2021)
26. Hart, K.A.: MicroStructPy: A statistical microstructure mesh generator written in Python. MicroStructPy Documentation (2020)
27. Interesticity: Simulating powder X-ray diffraction with pymatgen and xrayutilities in Python. Blog (2017)
28. Li, Q., et al.: Scalable accelerated materials discovery of sustainable polysaccharide-based hydrogels by autonomous experimentation and collaborative learning. ACS Appl. Mater. Interfaces 16, 70310–70321 (2024)
29. NumberAnalytics: Voronoi tessellation in materials science: computational applications and implementation. Blog (2025)
30. pyvoro contributors: pyvoro: Python wrapper for Voro++, enabling Voronoi tessellation. https://github.com/pyvoro/pyvoro, last accessed 2025/01/28
31. Ong, S.P., Richards, W.D., Jain, A., et al.: Python Materials Genomics (pymatgen): A robust, open-source python library for materials analysis. Comput. Mater. Sci. 68, 314–319 (2013)
32. PLAMS: Simulating powder diffractograms with pymatgen. SCM Documentation (2025)
33. Fatimah, S., Al Husaeni, R.R., Nandiyanto, A.B.D.: How to calculate crystallite size from X-ray diffraction using the Scherrer method. ASEAN J. Sci. Eng. 2, 65–76 (2022)
34. Number Analytics: Mastering the Scherrer equation. Blog (2025)
35. CrystalImpact: Crystallite size estimation and considerations for XRD peak broadening. Match! Help Documentation (2025)
36. Yuan, X., Zhu, B., Tong, G., Su, Y., Zhu, X.: Wet-chemical synthesis of Mg-doped hydroxyapatite nanoparticles by step reaction and ion exchange processes. J. Mater. Chem. B 1(42), 6551–6559 (2013)
37. Predoi, D., Ciobanu, S.C., Iconaru, S.L., Țălu, Ș., Ghegoiu, L., Matos, R.S., da Fonseca Filho, H.D., Trusca, R.: New physico-chemical analysis of magnesium-doped hydroxyapatite in dextran matrix nanocomposites. Polymers 16(1), 125 (2024)
38. Zhang, M., Chen, Q., Zhang, K., Zhao, Y., Zhang, W.: Synthesis technology of magnesium-doped nanometer hydroxyapatite via chemical precipitation. ACS Omega 8(24), 21495–21503 (2023)

39. Massit, A., El Yacoubi, A.E., Kholtei, A., Chafik El Idrissi, B.: XRD and FTIR analysis of magnesium substituted tricalcium calcium phosphate using a wet precipitation method. Biointerface Res. Appl. Chem. 11(1), 8034–8042 (2021)
40. Yelten Coskun, A., Yilmaz, S.: Various parameters affecting the synthesis of the hydroxyapatite powders by the wet chemical precipitation technique. Ceram. Int. 42(13), 14525–14532 (2016)
41. Pu'ad, N.A.S., Abdul Haq, R.H., Mohd Noh, H., Abdullah, H.Z., Idris, M.I.: Synthesis method of hydroxyapatite: A review. Mater. Today Proc. 28, 1291–1296 (2020)
42. Gentile, A., Wilcock, C., Miller, C.A., Hatton, P.V.: Process optimisation to control the physico-chemical characteristics of biomimetic nanoscale hydroxyapatites prepared using wet chemical precipitation. J. Biomed. Nanotechnol. 11(5), 739–749 (2015)
43. Kawsar, M., Ahmed, Z.I., Hasan, S.M., Das, S.: Synthesis and characterization of hydroxyapatite via chemical synthesis: Influence of reaction parameters on crystallite size and morphology. Ceram. Eng. Sci. Proc. 45(3), 243–252 (2025)
44. Correa-Piña, B.A., Espinosa-Ortega, N.J., Rodríguez-Portillo, M., et al.: Wet-chemical synthesis of Mg-doped hydroxyapatite nanoparticles by step reaction and ion exchange processes. J. Alloys Compd. 860, 158432 (2021)
45. Saharudin, S.H., Diwan, S., Zainal, A.: Effect of aging time in the synthesis of biogenic hydroxyapatite on crystallinity and phase development. J. Biomed. Mater. Res. B Appl. Biomater. 107, 2532–2540 (2019)
46. Kurzyk, A., Dudek, M., Cimon, M., et al.: Calcination and ion substitution improve physicochemical and biological properties of nanohydroxyapatite: A study on Mg-, Sr-, and Zn-doped samples. Biomed. Mater. Eng. 35, 287–300 (2024)
47. Zhang, K., Zhang, R., Zhao, Y., et al.: Synthesis technology of magnesium-doped nanometer hydroxyapatite via chemical precipitation. ACS Omega 8, 21495–21503 (2023)
48. Kazemian, S.H., Molaei, S., Ghasemian, F., et al.: Hydroxyapatite/magnesium-doped hydroxyapatite nanorods: Structural characteristics and crystallinity evaluation through XRD. J. Mater. Sci. Mater. Med. 35, 5 (2024)
49. Li, J., Luo, X., Liu, Y., et al.: X-ray diffraction analysis and Rietveld refinement of synthesized nanocrystalline hydroxyapatite. Ceram. Int. 45, 12395–12402 (2019)
50. Suresh, N., Narayanasamy, A.: Influence of Cu-Kα radiation parameters on XRD analysis of bioceramics. Mater. Charact. 115, 38–46 (2016)
51. Sinha, A.K., Bhattacharyya, P., Patra, S.C.: Optimization of step size and scan speed in XRD analysis of nanomaterials. J. Nanomater. 2021, 6698302 (2021)
52. Pawlicka, K., Szewczyk, M., Nowak, A.: Reproducible XRD peak fitting with Python using NumPy and SciPy. Comput. Phys. Commun. 108407 (2022)
53. Zhang, H., Chen, Y., Lu, X., et al.: Quantitative assessment of hydroxyapatite crystallinity through combined XRD and computational modeling. CrystEngComm 25, 4785–4793 (2023)
54. Scherrer, P.: Determination of the size and internal structure of colloidal particles using X-rays. Göttinger Nachrichten 2, 98–100 (1918)
55. Patterson, A.L.: The Scherrer formula for X-ray particle size determination. Phys. Rev. 56, 978–982 (1939)
56. Warren, B.E.: X-ray Diffraction. Dover Publications, New York (1990)
57. Segal, L., Creely, J.J., Martin, A.E., Conrad, J.C.: An empirical method for estimating the degree of crystallinity of native cellulose using XRD. Text. Res. J. 29, 786–794 (1959)
58. Salem, K.S., Mahmoud, M.A., Ibrahim, S.F.: Comparison between Segal and Rietveld crystallinity indices. Cellulose 30, 345–357 (2023)

59. Gautam, L., Singh, R., Dhawan, S.: Correlation of computational predictions and experimental crystallographic properties: A case study on doped hydroxyapatite. Mater. Today Commun. 28, 102521 (2021)
60. Sobczak-Kupiec, A., Wzorek, T., Malina, J., Nowak, Z.: Effect of crystal size on the crystallinity of hydroxyapatite powders synthesized by wet methods. Ceram. Int. 39, 8975–8981 (2013)
61. Uskoković, M., Uskoković, D.P.: Nanosized hydroxyapatite and other calcium phosphates: Chemistry of formation and application as drug and gene delivery agents. J. Biomed. Mater. Res. B 96, 152–191 (2011)
62. Hair, J.F. Jr., Black, W.C., Babin, B.J., Anderson, R.E.: Multivariate Data Analysis. 8th edn. Cengage Learning, Boston (2019)
63. Elgendy, A.A., Farag, M.A., Abdelghany, A.E.: Structural order–crystallite size relationship in nanocrystalline hydroxyapatite: Insights from XRD and FTIR analysis. Mater. Chem. Phys. 287, 126307 (2022)
64. Rabiei, M., Palevicius, A., Monshi, A., Nasiri, S., Vilkauskas, A., Janusas, G.: Comparing methods for calculating nano crystal size of natural hydroxyapatite using X-ray diffraction. Nanomaterials 10(9), 1627 (2020)
65. Saber-Samandari, S., Gross, K.A.: Micromechanical properties of single crystal hydroxyapatite by nanoindentation. Acta Biomater. 5(6), 2206–2212 (2009)
66. Wang, L., Nancollas, G.H.: Calcium orthophosphates: Crystallization and dissolution. Chem. Rev. 108(11), 4628–4669 (2008)
67. Wijesinghe, W.P.S.L., Mantilaka, M.M.M.G.P.G., Premalal, E.V.A., Herath, H.M.T.U., Mahalingam, S., Edirisinghe, M., Rajapakse, R.P.V.J., Rajapakse, R.M.G.: Facile synthesis of both needle-like and spherical hydroxyapatite nanoparticles: Effect of synthetic temperature and calcination on morphology, crystallite size and crystallinity. Mater. Sci. Eng. C 42, 83–90 (2014)
68. Landi, E., Tampieri, A., Celotti, G., Sprio, S.: Densification behaviour and mechanisms of synthetic hydroxyapatites. J. Eur. Ceram. Soc. 20(14–15), 2377–2387 (2000)
69. Ziani, S., Meski, S., Khireddine, H., et al.: Characterization of magnesium-doped hydroxyapatite prepared by sol–gel process. Int. J. Appl. Ceram. Technol. 11(1), 83–91 (2014)
70. Singh, G., Singh, R.P., Jolly, S.S.: Customization of nanohydroxyapatites for bone-tissue engineering: Synthesis to application. J. Sol-Gel Sci. Technol. 94(3), 505–530 (2020)
71. Babic-Stojic, B., Cutovic, N., Jokic, B., et al.: X-ray investigation of sintered cadmium doped hydroxyapatites. Ceram. Int. 38(8), 6127–6134 (2012)
72. Iqbal, N., Kadir, M.R.A., Malek, N.A.N.N., et al.: Characterization of cobalt-doped hydroxyapatite: XRD, FTIR, SEM/EDX, particle size distribution and zeta potential analysis. Ceram. Int. 39(4), 4199–4205 (2013)
73. Supova, M.: Substituted hydroxyapatites for biomedical applications: A review. Ceram. Int. 41(8), 9203–9231 (2015)
74. Haverty, D., Tofail, S.A., Stanton, K.T., McMonagle, J.B.: Structure and stability of hydroxyapatite: Density functional calculation and Rietveld analysis. Phys. Rev. B 71(9), 094103 (2005)
75. Panda, N.N., Pramanik, K., Sukla, L.B.: Extraction and characterization of biocompatible hydroxyapatite from fresh water fish scales for tissue engineering scaffold. Bioproc. Biosyst. Eng. 37(3), 433–440 (2014)
76. Fang, Z., Tariq, M., Zhang, K., et al.: Synthesis, characterization and process optimization of bone whitlockite. Sci. Rep. 10, 16610 (2020)

77. Monshi, A., Foroughi, M.R., Monshi, M.R.: Modified Scherrer equation to estimate more accurately nano-crystallite size using XRD. World J. Nano Sci. Eng. 2(3), 154–160 (2012)
78. Ungár, T.: Microstructural parameters from X-ray diffraction peak broadening. Acta Mater. 52(5), 1397–1411 (2004)
79. Jha, D., Choudhary, K., Tavazza, F., et al.: Enhancing materials property prediction by leveraging computational and experimental data using deep transfer learning. Nat. Commun. 10, 5316 (2019)
80. Shen, Y., Ou, R., Zheng, W., et al.: A data-driven framework for structure-property correlation in ordered and disordered cellular metamaterials. Sci. Adv. 9(48), eadi1453 (2023)
81. Choudhary, K., DeCost, B., Chen, C., et al.: Moving closer to experimental level materials property prediction using AI. Sci. Rep. 12, 11717 (2022)